Nuclear Engineering and Technology 55 (2023) 1342–1349

Contents lists available at ScienceDirect

Nuclear Engineering and Technology

journal homepage: www.elsevier.com/locate/net

Original Article

Feasibility study of using triple-energy CT images for improving stopping power estimation

Yejin Kim [a], Jin Sung Kim [b], Seungryong Cho [a, c, *]

[a] Department of Nuclear and Quantum Engineering, Korea Advanced Institute of Science and Technology, Daejeon, Republic of Korea
[b] Department of Radiation Oncology, Yonsei Cancer Center, Yonsei University Health System, Yonsei University College of Medicine, Seoul, Republic of Korea
[c] KAIST Institutes for Health Science and Technology and ICT Convergence, Korea Advanced Institute of Science and Technology, Daejeon, Republic of Korea

ARTICLE INFO

Article history:
Received 6 September 2022
Received in revised form
14 December 2022
Accepted 15 December 2022
Available online 15 December 2022

Keywords:
Charged particle therapy
Stopping power
Multi-energy CT

ABSTRACT

The planning accuracy of charged particle therapy (CPT) is subject to the accuracy of stopping power (SP) estimation. In this study, we propose a method of deriving a pseudo-triple-energy CT (pTECT) that can be achievable in the existing dual-energy CT (DECT) systems for better SP estimation. In order to remove the direct effect of errors in CT values, relative CT values according to three scanning voltage settings were used. CT values of each tissue substitute phantom were measured to show the non-linearity of the values thereby suggesting the absolute difference and ratio of CT values as parameters for SP estimation. Electron density, effective atomic number (EAN), mean excitation energy and SP were calculated based on these parameters. Two of conventional methods were implemented and compared to the proposed pTECT method in terms of residuals, absolute error and root-mean-square-error (RMSE). The proposed method outperformed the comparison methods in every evaluation metrics. Especially, the estimation error for EAN and mean excitation using pTECT were converging to zero. In this proof-of-concept study, we showed the feasibility of using three CT values for accurate SP estimation. Our suggested pTECT method indicates potential clinical utility of spectral CT imaging for CPT planning.

1. Introduction

Charged particle beam therapy field is rapidly growing in both technological and clinical aspects worldwide for its physical and biological advantages over photon therapy [1,2]. Charged particle therapy uses heavy particles such as protons, neutrons, and helium or carbon ions exploiting their high linear energy transfer (LET) characteristics [3]. Peculiar depth-dose characteristics of energetic charged particle represented by Bragg's peak [4] provide the major physical advantage for cancer therapy with their efficient dose coverage of the target tumor and marginal exit dose [5].

In order to make the best use of Bragg's peak, it is crucial to precisely control the range of the beam which depends not only on the beam characteristics but also on the physical properties of the target human body [6]. One of the main challenges in charged particle therapy is the treatment planning uncertainty [7,8]. For the treatment planning, tomographic information of stopping power (SP) of human body is necessary. SP is dependent on electron density, effective atomic number (EAN), and mean excitation energy of the tissues. In general, single-energy x-ray computed tomography (CT) is used for estimating the tomographic information of SP for the human body. One of the most popularly used methods for converting the Hounsfield Unit (HU), i.e., CT number, to SP for particle therapy was proposed in 1996 by Schneider [9], which is still in active use in most clinical sites. This method uses a stoichiometric calibration, which models the dependence of the photon attenuation as a function of the atomic number of the elemental composition of tissue substitutes with their known chemical composition. This conventional method correlates the CT numbers in a one-to-one manner to the particle's stopping powers via the so-called Hounsfield look-up table (HLUT).

However, conventional single-energy CT (SECT) uses an x-ray tube that generates photon beam with a broad spectrum of energies. The polychromatic photons induce image artifacts, although artifacts correction is made to a certain degree, in the reconstructed CT images possibly making it difficult to estimate the SP [10]. Also, the fundamental physical differences in the interactions of photons and charged particles with matters introduce errors for estimating SP directly from SECT [11].

* Corresponding author. Department of Nuclear and Quantum Engineering, Korea Advanced Institute of Science and Technology, Daejeon, Republic of Korea.
E-mail address: scho@kaist.ac.kr (S. Cho).

https://doi.org/10.1016/j.net.2022.12.018

In an effort to overcome this, a variety of CT-based methods have been developed including dual-energy CT based approaches for more accurate SP estimation for treatment planning of particle therapy [12–19]. It is consistently reported that the DECT outperforms the HLUT-based conventional SECT in predicting the electron density relative to water (ED) regardless of the algorithms. However, predicting the mean excitation energy still has room to be improved and it is noted that ED and mean excitation energy are both critically important for calculating SP via the Bethe's formula [20].

While DECT has been increasingly investigated for various clinical uses, spectral photon-counting CT (SPCCT) is under an active research and development with its potential to be a game-changer for clinical CT [21]. SPCCT uses photon counting detectors, which count the number of incoming photons and measure each of their energies unlike the conventional energy-integrating detectors. SPCCT has been reported to yield higher spatial resolution, less imaging artifact, and improved contrast-to-noise ratio [22]. Even though considerably high cost of SPCCT is a main impediment for adopting the technology widely to the clinics yet, SPCCT is considered to be the future of clinical CT and expected to provide better solution to reducing the range uncertainties for charged particle therapy planning as well. To our knowledge, there is no study of using SPCCT with its multiple-energy resolving power for charged particle therapy planning.

Unlike photon-based imaging, particle imaging such as proton CT provides direct calculation of particle stopping power and is under active research for the past decade. Among particle imaging methods, proton imaging is the most promising, multiple prototype system available worldwide in research institutions [23,24,25]. However, the limited image quality of proton CT compared to the X-ray CT due to Coulomb scattering hinders the fast translation of proton CT to clinical setup. Helium imaging is also considered a complement to photon-based imaging, yet is in the early phase of research only [26].

As SPCCT is not yet ready for its routine use in the treatment planning in charged particle therapy but is of great potential, we wanted to provide a bridging study that motivates use of multi-energy imaging capability of the SPCCT in the future. In this study, we show the feasibility of a pseudo-triple energy CT (pTECT) imaging for estimating more accurate SP for charged particle therapy planning than DECT. Pseudo-TECT uses a commercial DECT system and acquires an additional single-energy CT image from a separate scan on top of the dual-energy images thus comprising triple-energy setting. The x-ray energy spectra of the aforementioned triple-energy setting would have intrinsic overlap each other unlike the ideal energy-bin based spectral separation in SPCCT. Therefore, we named the scanning approach used in this work a pseudo-triple energy CT. There could be a concern on the additional patient imaging dose due to double-scan. However, we would like to note that the double-scan based pTECT acquisition is a preliminary way for acquiring triple energy CT, and can be replaced by a single-scan multiple-energy CT such as photon-counting detector (PCD) CT when its technology becomes mature. The performance of SP estimation by use of the pTECT is compared to those of conventional SECT and DECT based SP estimations.

2. Materials and methods

2.1. Phantom

For the validation experiment, Gammex 467, a tissue characterization phantom, was used. Gammex 467 phantom consists of a solid water disk with its size of approximately an average pelvis (33 cm) and multiple tissue substitute rods. A matrix of sixteen holes in the disk have rods of tissue-simulating materials including solid water, lung, adipose, breast, and bone. The ED, physical density, and expected CT number of the materials in the phantom are provided by the vendor.

2.2. Pseudo-triple energy CT image acquisition

For CT image acquisition, tube voltage settings of 80/140 kVp without a filter and 80/150 kVp with a tin filter for 150 kVp using SOMATOM Force, a dual-energy CT scanner by Siemens Healthineers, were used. Among these four sets of CT images, three images from 80, 140 and 150 (with a tin filter) kVp were used to demonstrate the validity of the proposed method.

The CT number of a single material may vary according to the scanning conditions especially including the x-ray tube voltage (Please see Fig. 1). For example, a rod of cortical bone substitute in the phantom is known to have CT numbers of 1602.0, 1360.6, 1188.6 and 1092.0 at 80, 100, 120 and 140 kVp scanning conditions respectively (Table 1). This difference in CT numbers is not linear to the tube voltage, nor has a clear tendency. Indeed, the nonlinear response of the CT number to the tube voltage can be used for material decomposition, or for identifying the ED, EAN and mean excitation energy as is done in this work.

Experimental setup and the CT image slice of the phantom are shown in Fig. 2. Among sixteen human tissue substitute rods of the Gammex 467, five of them are solid waters and identical to the phantom disk. Therefore, there are twelve different tissue mimicking rods and physical properties of each material are summarized in Table 2, which came from the user guide book of Gammex 467 and Table 1 from Bourque's paper (2014) [15]. In order to measure CT number of each material experimentally in this work, a volume-of-interest (VOI) composed of $10 \times 10 \times 10$ voxels of each rod was selected in the reconstructed image domain and an averaged CT value of the VOI was used (Fig. 2B). Hence, we have three sets of CT numbers for twelve tissues, $CT_L = \{CT_L^1, CT_L^2, \ldots, CT_L^{12}\}$, $CT_M = \{CT_M^1, CT_M^2, \ldots, CT_M^{12}\}$, and $CT_H = \{CT_H^1, CT_H^2, \ldots, CT_H^{12}\}$ where the subscript letters L, M and H denote the low, medium, and high tube voltages (80, 140 and 150 kVp respectively from DECT scanning in this paper) and the superscript numbers from 1 to 12 denote different tissue substitutes of the phantom. We would like to note that we use the reduced CT number, as defined in the following, throughout the paper and also introduce difference parameters, D_1 and D_2, as following for each material:

$$CT_{reduced} = \frac{CT_{measured} + 1000}{1000} \tag{1}$$

$$D_1 = \frac{CT_L - CT_M}{CT_M - CT_H} \tag{2}$$

$$D_2 = CT_M - CT_H \tag{3}$$

The parameters, D_1 and D_2, will be used as inputs for calculating ED and EAN.

For the SECT scanning, x-ray tube energy of 140 kVp by SOMATOM Sensation Open by Siemens Healthineers was used to demonstrate Schneider's method. For the DECT scanning, 80/150 kVp with a tin filter setting, that was used in the pTECT scan, was employed.

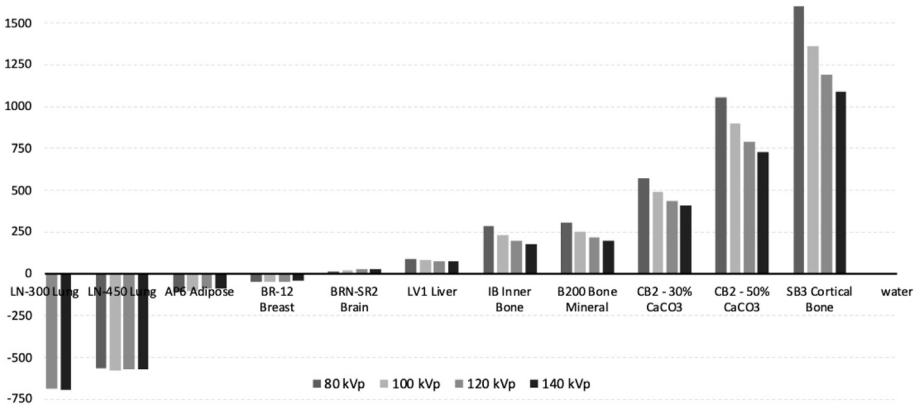

Fig. 1. CT numbers of rod materials according to the x-ray tube voltages as measured with a GE CT/iTM scanner by the Gammex 467 phantom manufacturer. The difference in CT numbers for each material is not linear to different tube voltages nor has clear relation to it.

Table 1
CT number of cortical bone substitute rod by Gammex 467. Given CT numbers of the tissue substitutes are given by the manufacturer measured with a *GE CT/i*™ scanner.

X-ray tube energy in kVp	80	100	120	140
CT number of Cortical Bone	1602.0	1360.6	1188.6	1092.0

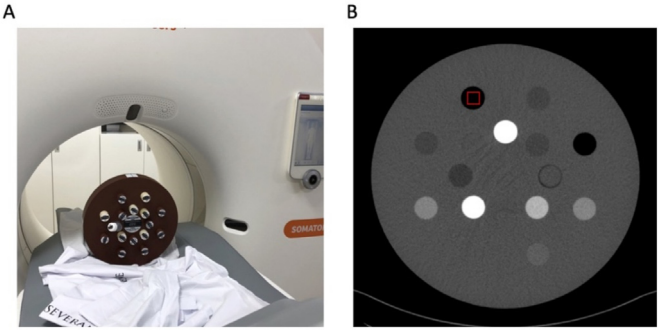

Fig. 2. (A) Scanning of Gammex 467 phantom using SOMATOM Force by Siemens Healthineers. (B) Reconstructed image of the phantom. The red box indicates the voxel selection example for calculating measured CT number for each rod. (For interpretation of the references to colour in this figure legend, the reader is referred to the Web version of this article.)

Table 2
Physical properties of Gammex 467 materials provided by the manufacturer and Table 1 of A.E. Bourque's paper (2014).

Rod Name (Abbreviation)	ρ_e^{rel}	Z_{ref}	I_{ref}
SB3 Cortical Bone (CortB)	1.69	13.51	104.5
BRN-SR2 Brain (Brain)	1.04	6.04	63.5
AP6 Adipose (Adipose)	0.93	6.17	66.6
CB2 Resin 50% $CaCO_3$ (CB2 50)	1.47	12.4	93.2
CB2 Resin 30% $CaCO_3$ (CB2 30)	1.28	10.76	80.7
CT Solid Water (Water)	0.99	7.66	70.4
BR-12 Avg. Breast (Breast)	0.96	6.87	68.2
LN-300 Lung (Lung300)	0.29	7.55	73.9
IB Inner Bone (Inner Bone)	1.09	10.28	80.1
LV1 Liver (Liver)	1.06	7.66	70.3
B200 Bone Mineral (B200)	1.10	10.29	80.2
LN-450 Lung (Lung450)	0.44	7.52	73.8

2.3. Basic physics for electron density, EAN, mean excitation energy and SP

$$(\text{Stopping Power}) = \rho_e^{rel}\frac{k_0 z^2}{\beta^2}\left[\ln\left(\frac{2m_e c^2\beta^2}{I\bullet(1-\beta^2)}\right)-\beta^2\right] \tag{4}$$

According to the Bethe's formula, stopping power is proportional to both electron density relative to water (ED), ρ_e^{rel}, and negative of logarithm of mean excitation energy, $-\ln(I)$. Here, β, k_0, z, m_e, and c represent particle velocity relative to the speed of light in vacuum, constant number 0.17045 MeV/cm, charge of the particle (*e.g.*, 1 for proton beam), rest mass of the electron, and the speed of light respectively. The ED and mean excitation energy, which finally are used as inputs for Bethe's formula for SP prediction, are calculated via polynomial fitting. The physical definition of ED is:

$$\rho_e = \rho_{mass} N_A \left(\frac{Z}{A}\right)_{eff} \tag{5}$$

, where ρ_{mass} and N_A are mass density in g/cm^3 and Avogadro's constant in mol^{-1} respectively. The chemical composition is

$$\left(\frac{Z}{A}\right)_{eff} = \sum_i P_i\left(\frac{Z_i}{A_i}\right) \tag{6}$$

, where P_i indicates the fraction by weight of the i th element (atomic number Z_i with mass number A_i) in the material.

The electron density relative to water is calculated as following:

$$\rho_e^{rel} = \frac{\rho_e}{\rho_w} = \frac{\rho_{mass}\left(\frac{Z}{A}\right)_{med,eff}}{\rho_{mass,w}\left(\frac{Z}{A}\right)_{w,eff}} \tag{7}$$

, where ρ_w is electron density of water, and $\rho_{mass,w}$ is mass density of water which is 1.

According to Schneider et al. (1996), who suggested stoichiometric calibration that is being used worldwide, for a given energy spectrum, the attenuation coefficient of a mixture of elements relative to water (μ) can be calculated as following [9]:

$$\mu = \rho_e^{rel}\left\{k_{ph}Z^{3.62} + k_{coh}Z^{1.86} + k_{KN}\right\} \tag{8}$$

, where the value of Z^m is obtained from the known chemical composition of medium with the following formula:

$$Z^m = \left[\sum_i \omega_i Z_i^m\right]^{\frac{1}{m}} \tag{9}$$

with m representing 3.62 or 1.86. The coefficients k_{ph}, k_{coh} and k_{KN} represent the cross-sections of photoelectric effect, coherent scattering and incoherent scattering respectively. The value of ω_i is determined by

$$\omega_i = \frac{P_i\left(\frac{Z_i}{A_i}\right)}{\left(\frac{Z}{A}\right)_{eff}} \tag{10}$$

Here, i considers each element of the material. By measuring the CT number of each tissue substitute materials with its known chemical composition in the fixed energy setting, one can easily determine the coefficients k_{ph}, k_{coh} and k_{KN} using a linear regression fit.

2.4. Calculation of ED, EAN, mean excitation energy and SP

In this study, we use the parameters D_1 and D_2 for each material which are defined above instead of using the CT numbers directly. Given that the effective atomic number of a material is decided by measured CT numbers in the end, we can simply express the effective atomic number by means of polynomial expansion using D_1 and D_2:

$$\boldsymbol{Z}_{mat} = \mathbf{D}\boldsymbol{c} \tag{11}$$

, where $\boldsymbol{Z}_{mat}$ is a vector consisting of EAN of each material, $\mathbf{D}$ is a parameter matrix and $\boldsymbol{c}$ is a vector for polynomial coefficients. More specifically, $\mathbf{D}$ is expressed by following:

$$\mathbf{D} = \left(\begin{array}{cccc|cccc} 1 & D_{1,1} & D_{1,1}^2 \cdots & D_{1,1}^{l-1} & 1 & D_{2,1} & D_{1,1}^2 \cdots & D_{2,1}^{l-1} \\ 1 & D_{1,2} & D_{1,1}^2 \cdots & D_{1,2}^{l-1} & 1 & D_{2,2} & D_{2,1}^2 \cdots & D_{2,2}^{l-1} \\ & & \vdots & & & & \vdots & \\ 1 & D_{1,N} & D_{1,N}^2 \cdots & D_{1,N}^{l-1} & 1 & D_{2,N} & D_{2,N}^2 \cdots & D_{2,N}^{l-1} \end{array}\right) \tag{12}$$

, where $D_{1,n}$ and $D_{2,n}$ represent the rational and length parameters for the material n defined in the pseudo-triple energy CT image acquisition. In this study, we have twelve tissue substitute materials in the Gammex phantom, therefore $N = 12$. Also, l represents the accuracy level of polynomial expansion, which is empirically fixed to 6 in this study. The polynomial coefficient vector $\boldsymbol{c}$ is defined by:

$$\boldsymbol{c} = \begin{pmatrix} c_{1,1} \\ c_{1,2} \\ \vdots \\ c_{1,l} \\ \\ c_{2,1} \\ c_{2,2} \\ \vdots \\ c_{2,l} \end{pmatrix} \tag{13}$$

Here, the vector $\boldsymbol{c}$ can be determined by least square solution using the known values from the phantom:

$$\boldsymbol{c} \approx \left(\mathbf{D}^T\mathbf{D}\right)^{-1}\mathbf{D}^T\boldsymbol{Z}_{phantom} \tag{14}$$

The matrix $\mathbf{D}$ is measured and the vector of EAN $\boldsymbol{Z}_{phantom}$ is known for the given phantom. Having the polynomial coefficient vector, one can easily obtain the EAN $\boldsymbol{Z}_{mat}$ using the formulae above.

It is known that there exists a correlation between the mean excitation energy (I) and EAN. However, there is no clear relationship between the two for some media, especially for human tissues. Therefore, we parametrize the I value as a function of the EAN for our human tissue substitutes with a form of polynomial function as follows:

$$I = \begin{cases} e_1 Z + e_2 & for\ Z < Z_{min} \\ e_3 Z^3 + e_4 Z^2 + e_5 Z + e_6 & for\ Z_{min} \le Z \le Z_{max} \\ e_7 Z + e_8 & for\ Z_{max} < Z \end{cases} \tag{15}$$

In this equation, the third order polynomial in the middle is determined by least squares fit using the known values of the phantom and the other two linear expressions are determined to be continuous with the third order polynomial in the middle, assuming a linear form beyond threshold values Z_{min} and Z_{max}.

Similarly, the calculation of ED can be done in the pTECT framework. As mentioned above, it is known that the electron density relative to water is obtained from the effective atomic number, thus correlated to the CT number. That is, the conventional expression of electron density by Schneider can be rewritten by:

$$\mu = \rho_e^{rel}\sum_{i=1}^{m} k_i Z^{i-1} \tag{16}$$

, where m and k_i denote the highest order used in the polynomial approximation and the expansion coefficients respectively. This can be represented by matrix form as following:

$$\boldsymbol{\mu} = \boldsymbol{RZK} \tag{17}$$

, where $\boldsymbol{\mu}$ is a $N \times 1$ column vector consisting of the measured attenuation coefficients from different tissue substitute materials, and $\boldsymbol{R}$ is a $N \times N$ diagonal matrix with given EDs from the phantom information as following:

$$\boldsymbol{R} = \begin{pmatrix} \rho_{e,1}^{rel} & 0 & \cdots & 0 \\ 0 & \rho_{e,2}^{rel} & \cdots & 0 \\ \vdots & \vdots & \ddots & \vdots \\ 0 & 0 & 0 & \rho_{e,N}^{rel} \end{pmatrix} \tag{18}$$

$\boldsymbol{Z}$ is a polynomial expression of calculated EAN values $\boldsymbol{Z}_{mat}$:

$$\boldsymbol{Z} = \begin{pmatrix} 1 & Z_{mat,1} & Z_{mat,1}^2 \cdots & Z_{mat,1}^{m-1} \\ 1 & Z_{mat,2} & Z_{mat,2}^2 \cdots & Z_{mat,2}^{m-1} \\ & & \vdots & \\ 1 & Z_{mat,N} & Z_{mat,N}^2 \cdots & Z_{mat,N}^{m-1} \end{pmatrix} \tag{19}$$

Finally, $\boldsymbol{K}$ is a column vector of polynomial coefficients k_i:

$$\boldsymbol{K} = \begin{pmatrix} k_1 \\ k_2 \\ \vdots \\ k_m \end{pmatrix} \tag{20}$$

Again, we have twelve different tissue substitutes, so $N = 12$. The highest order used in the polynomial estimation m is determined to be 6 empirically. Here, the values for $\boldsymbol{K}$ can be determined by least square solution:

$$\boldsymbol{K} \approx \left((\boldsymbol{RZ})^{\boldsymbol{T}}\boldsymbol{RZ}\right)^{-1}(\boldsymbol{RZ})^{\boldsymbol{T}}\boldsymbol{\mu} \tag{21}$$

with the calculated $\boldsymbol{Z}$ and given $\boldsymbol{R}$. Then, the equation to get calculated $\boldsymbol{R}$ can be reformulated as:

$$\boldsymbol{R} = \boldsymbol{\mu} \oslash \boldsymbol{ZK} \tag{22}$$

, where operator $\oslash$ represents element-wise division of vectors. Here, we have three different attenuation coefficients from three energy spectra for each material, thereby resulting in three different EDs for each material. We took an average of the three EDs at the end.

2.5. Validation

For validation, residuals of ED, Z, mean excitation energy and SP for each material were calculated as following:

$$residual_i\ (\%) = \frac{\left|Var^i_{measured} - Var^i_{ref}\right|}{Var_{ref}} \times 100 \tag{23}$$

, where Var^i_{ref} is the reference variable value calculated from the known properties of the phantom material i and $Var^i_{measured}$ is the estimated value from the measurement.

Absolute error and root-mean-square-error (RMSE) of all the residuals derived from the proposed model were compared to those from SECT and DECT methods.

$$Absolute\ error_i = \left|Var^i_{measured} - Var^i_{ref}\right| \tag{24}$$

$$RMSE = \sqrt{\frac{\sum_{i=1}^{N}(Absolute\ error_i)^2}{N}} \tag{25}$$

3. Results

Measured CT numbers for the three tube voltage settings are shown in Fig. 3. Materials of relatively low CT numbers show less variation in CT numbers against tube voltages. On the contrary, the variation in CT numbers becomes large in relatively high density objects. Measured CT numbers are compared to the vendor-provided values from the phantom guide book for high (150 kVp) and low (80 kVp) tube voltages as shown in Fig. 4. Materials with low CT numbers show acceptable agreement between the measured and the provided values. However, materials with high CT numbers such as cortical bone and CB2 50 substantially deviate from the vendor-provided values, which is mostly due to the scanner specifics.

Overall, the estimated ED(ρ_e^{rel}), EAN(Z), mean excitation energy and finally the SP values were consistently improved in the results by the proposed method compared to the SECT and the DECT methods as shown in Table 3. Estimated EANs especially have significant improvement for most of materials showing average residuals of 8.37%, 1.64% and 0.11% and the maximum residuals 25.92%, 6.85% and 0.63% for the SECT, DECT and pTECT methods, respectively. Since the accuracy of mean excitation energy is largely affected by that of EAN, the residuals for EANs propagate to the those of mean excitation energies. On the other hand, the accuracy of estimated EDs is slightly improved compared to the SECT and DECT methods. High attenuation materials such as cortical bone and CB2 Resin 50% $CaCO_3$ are particularly subject to errors, showing residuals of 0.02 and 0.20 for SECT and 0.06 and 0.06 for DECT, respectively. However, the proposed method drastically reduces the residuals to 0.007 and 0.02 for these materials.

Absolute error of EDs, EANs, mean excitation energies, and SPs from the SECT, DECT and pTECT are summarized in Fig. 5 in the form of a box plot. The pTECT method outperformed the others in the entire estimated metrics in terms of both average and standard deviation. Resulting RMSEs of stopping powers relative to water are summarized in Table 4, indicating the decreased error from 1.1% to 0.1%–0.03% for SECT, DECT and pTECT, respectively.

4. Discussion

This paper shows the feasibility of using multi-energy-resolving CT for estimating the stopping power more accurately for charged particle therapy planning. We first showed that the SECT image has

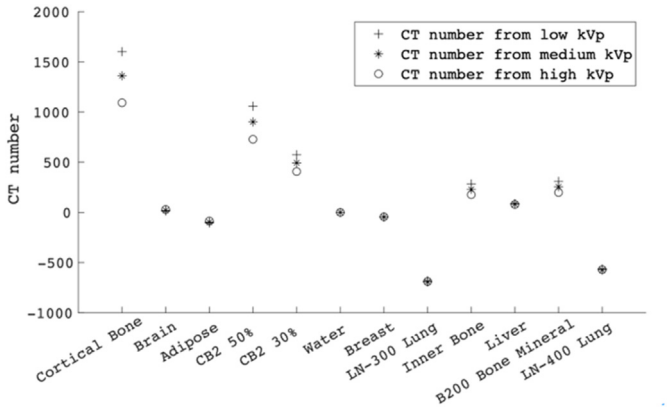

Fig. 3. Measurement of CT numbers for low, medium and high tube voltage settings (80, 140 and 150 kVp in this study).

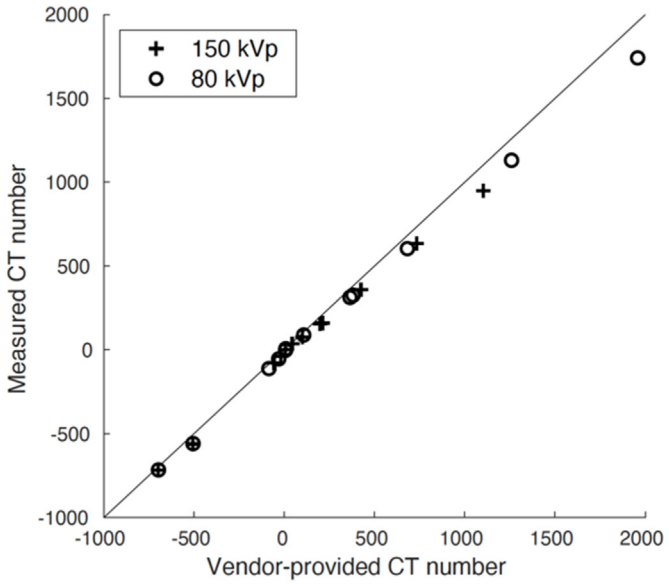

Fig. 4. Comparison of vendor-provided and measured CT numbers for high (150 kVp) and low(80 kVp) energy.

Table 3
Residuals of electron density relative to water (no unit, ED), atomic number (no unit, Z), mean excitation energy(eV, I) and stopping power (MeV/cm, SP) for SECT, DECT and our proposed pTECT method.

SECT					DECT					pTECT (proposed)				
material	ED	*Z*	*I*	SP	material	ED	*Z*	*I*	SP	material	ED	*Z*	*I*	SP
CortB	0.91	1.83	3.96	0.45	**CortB**	0.36	0.13	7.03	1.14	**CortB**	0.02	0.00	0.03	0.02
Brain	1.38	25.92	18.00	3.17	**Brain**	0.20	4.76	1.10	0.32	**Brain**	0.65	0.00	1.55	0.48
Adipose	1.32	11.37	5.41	1.89	**Adipose**	0.84	0.41	6.38	0.13	**Adipose**	0.73	0.00	2.13	0.49
CB2 50	3.12	7.40	12.09	4.38	**CB2 50**	1.47	0.26	0.30	1.44	**CB2 50**	0.15	0.00	0.26	0.18
CB2 30	0.58	0.79	2.46	0.85	**CB2 30**	0.83	0.31	2.81	1.14	**CB2 30**	0.68	0.00	1.47	0.84
Water	0.37	0.94	1.97	0.15	**Water**	0.09	0.01	1.47	0.26	**Water**	0.67	0.00	3.43	0.28
Breast	0.09	3.84	5.98	0.55	**Breast**	0.56	1.08	3.85	0.14	**Breast**	0.16	0.00	1.92	0.37
Lung300	3.68	5.38	3.11	4.00	**Lung300**	2.57	1.89	0.09	2.58	**Lung300**	3.17	0.00	0.97	3.06
Inner Bone	5.40	14.11	2.83	5.74	**Inner Bone**	0.51	0.19	1.07	0.63	**Inner Bone**	0.49	0.00	0.68	0.57
Liver	0.46	3.69	8.33	0.43	**Liver**	0.85	3.31	8.20	0.02	**Liver**	1.06	0.00	4.77	0.54
B200	5.19	13.22	2.79	5.53	**B200**	1.08	0.45	1.12	1.20	**B200**	0.20	0.00	0.75	0.29
Lung450	1.40	11.92	8.17	2.36	**Lung450**	0.01	6.85	3.36	0.39	**Lung450**	0.87	0.00	1.02	0.75
Average	1.99	8.37	6.26	2.46	**Average**	0.78	1.64	3.07	0.78	**Average**	0.74	0.00	1.58	0.66
Max	5.40	25.92	18.00	5.74	**Max**	2.57	6.85	8.20	2.58	**Max**	3.17	0.00	4.77	3.06

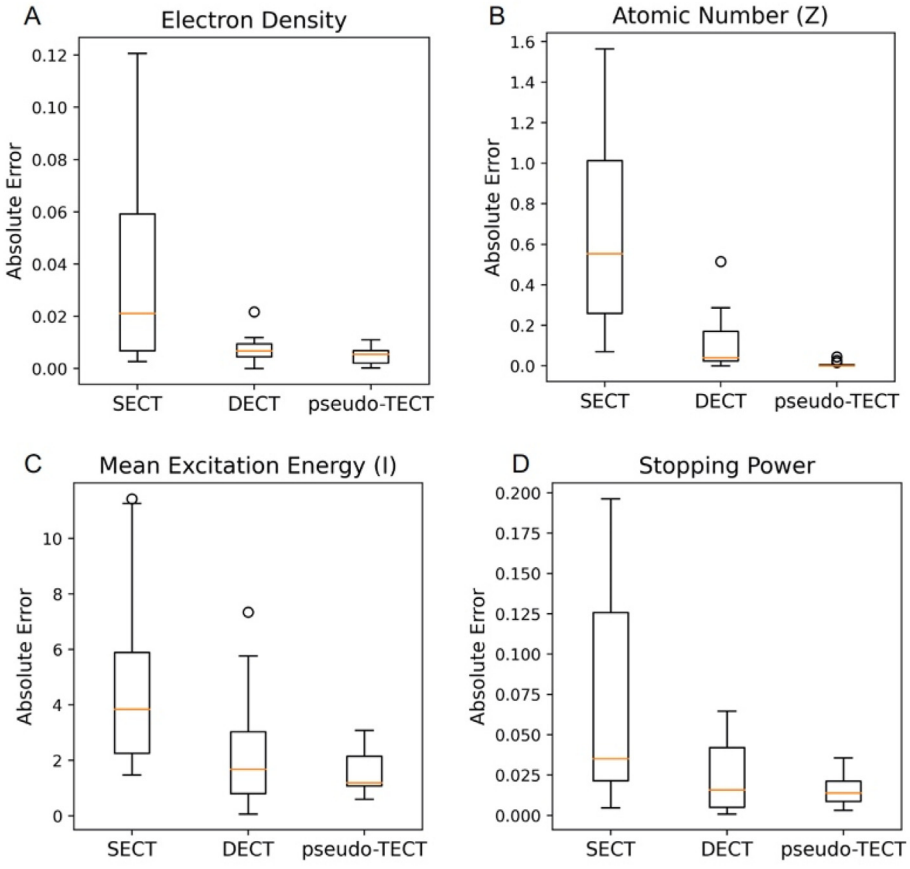

Fig. 5. Absolute errors of electron density (A), atomic number (B), mean excitation energy (C) and stopping power (D) from SECT, DECT and our proposed pTECT methods for twelve materials. The units of y-axis for each panel are eV (C), MeV/cm (D), and no unit for (A) and (B).

Table 4
Root mean square error times 100 of estimated stopping powers using SECT, DECT and out proposed pTECT methods.

	SECT	DECT	pTECT (proposed)
RMSEx100 of SP	1.1	0.1	0.03

inevitable uncertainties related to the selected tube voltage variation.

The error in SECT image would directly affect the SP estimation when using the conventional one-to-one look-up table method relating CT number with SP. Since the interactions of charged particles with matters are physically totally different from those of photons, such a one-to-one correspondence would not constitute a reliable SP estimation even if the CT number errors are corrected. In other words, there exist tissues that have the same or similar CT numbers but substantially different particle stopping powers.

DECT exploits nonlinear responses of the tissue to the x-ray beam spectra helping to reduce SP estimation uncertainties. From DECT, one can derive electron density and effective atomic number information of the tissue based on which SP map can be constructed for a given beam of charged particle. The proposed pTECT adds more information to DECT allowing even more accurate SP estimation. It should be noted that the proposed method uses relative ratio of the CT numbers instead of directly using the CT numbers only, which makes the method more robust against CT number variations. Residuals, absolute errors and RMSEs were evaluated and the proposed method outperformed the other two in every evaluation metrics. In this work, we used a linear algebraic approach to solving for EAN and ED by use of a set of empirical calibration data. There may exist other methods, possibly superior to the linear algebraic approach, for acquiring those from the measurements, but we believe that it is beyond the scope of this work.

In the first glance, our proposed method could be misinterpreted to imbed inverse crime, yet we clarify that the linear algebraic parameters are fitted using ground truth values of the human mimic phantom with known chemical compositions.

M. Witt et al., and F.K. Logarino et al. have investigated the effect of change in stopping power to the range shift [27,28]. According to study by M. Witt, 0.5% change in the stopping-power-ratio results in a deviation of particle ranges of 1 mm in 20 cm depth [27]. In the study of F.K. Logarino, the relative (absolute) proton range shifts of 0.6% (0.4 mm) in the mean and up to 4.4% (2.1 mm) at the distal fall-off in the plans of heterogeneous anatomies [28]. Further investigation of the benefits of the proposed method in the range verification will be conducted as our future study.

On the other hand, one may argue that the improvement in SP estimation accuracy of the pTECT is rather marginal compared to that of DECT. However, we would like to emphasize that not only the mean error but also its standard deviation has been substantially reduced in the pTECT as shown in Fig. 5. More importantly, as summarized in Table 3, the estimation error by the proposed method is particularly lower in high EAN materials such as cortical bone, CB2 resin 50% and 30% $CaCO_3$. Depending on the target tumor types and surrounding organ-at-risks (OARs), advantages of such a reduction in errors may become manifest in clinical applications. The clinical impacts of the proposed method should be investigated through a dosimetric validation study in a given charged particle therapy setting, and it remains as our future work.

We would like to note that the residuals in Table 3 are in absolute % error. pTECT showed lower residuals compared to the DECT and SECT in general with the average SP residuals of 2.46, 0.78, and 0.66 for SECT, DECT and pTECT respectively. However, in the cases of the soft tissues such as brain, adipose, breast, lung and liver, the result from pTECT showed slightly inferior performance compared to that from the DECT. On the other hand, in the cases of high-density materials such as CortB, CB2s, and B200, the use of pTECT led to a substantial improvement in the accuracy.

CT number uncertainty usually increases as the density of the object becomes high. Therefore, DECT typically shows a relatively high residual errors particularly for the high-density materials. However, since the pTECT uses the ratios of the CT numbers, the overall uncertainty tends to be smaller resulting in higher accuracy of SP in such high-density materials. Meanwhile, such an advantage is not guaranteed for the low-density materials since the reduction of residual errors due to the use of ratios of the triple energy CT numbers is not quite straightforward.

We would like to point out, however, that the accuracy of stopping-power estimation is also important in lower-density regions because many researchers reported that the dosimetric uncertainty in commercial treatment planning system (TPS), especially for particle therapy, is high in heterogeneous regions including lung regions. This might be related to the respiratory motion artifacts, the usage of contrast medium or not, and the Poisson noise level of the reconstructed CT images. Therefore, in our future study, we will address these issues for a more accurate estimation of stopping power with the CT images, ultimately, for the better quality of particle therapy.

We would also like to note that the proposed pTECT would come with an additional imaging radiation dose to the patient in its current shape. Although its practical use for charged particle therapy planning, therefore, would need a benefit-risk analysis, the focus of this work is rather on demonstrating the utility of using multiple-energy information which would hopefully be achieved by SPCCT at a dose-neutral condition in the future.

5. Conclusion

This paper shows the feasibility of using multi-energy-resolving CT for estimating the stopping power of charged particles. A substantial instability in CT values according to CT scanners is shown using human tissue mimic phantom, which implies the hazard of using raw CT numbers for stopping power estimation. Pseudo-Triple Energy CT (pTECT), our proposed method, is acquired using commercial DECT and suggests that rational and absolute difference of CT values for the same material in various CT tube voltage settings could perform better for stopping power estimation.

Declaration of competing interest

The authors declare that they have no known competing financial interests or personal relationships that could have appeared to influence the work reported in this paper.

Acknowledgement

This study is supported in part by the National Research Foundation of Korea Grant NRF-2020R1A2C2011959, the Institute of Civil Military Technology Cooperation funded by the Defense Acquisition Program Administration and Ministry of Trade, Industry and Energy of Korean government under grant UM19207RD2, and the National Research Foundation of Korea Grant NRF-2021M3I1A109790911.

References

[1] H. Paganetti, C. Beltran, S. Both, L. Dong, J. Flanz, K. Furutani, C. Grassberger, D.R. Grosshans, A.C. Knopf, J.A. Langendijk, H. Nystrom, K. Parodi, B.W. Raaymakers, C. Richter, G.O. Sawakuchi, M. Schippers, S.F. Shaitelman, B.K.K. Teo, J. Unkelbach, P. Wohlfahrt, T Lomax, Roadmap: Proton therapy physics and biology, Phys. Med. Biol. 66 (5) (2021).
[2] T.D. Malouff, A. Mahajan, S. Krishnan, C. Beltran, D.S. Seneviratne, D.M. Trifiletti, Carbon ion therapy: a modern review of an emerging technology, Front. Oncol. 10 (82) (2020).
[3] D.T. Goodhead, Mechanisms for the biological effectiveness of high-LET radiations, J. Radiat. Res. 40 (1999) 1–13.
[4] A. Brown, H. Suit, The centenary of the discovery of the Bragg peak, Radiother. Oncol. 73 (3) (2004) 265–268.
[5] C. Grassberger, H. Paganetti, Elevated LET components in clinical proton beams, Phys. Med. Biol. 56 (20) (2011) 6677–6691.
[6] A. Besemer, H. Paganetti, B. Bednarz, The clinical impact of uncertainties in the mean excitation energy of human tissues during proton therapy, Phys. Med. Biol. 58 (4) (2013) 887–902.
[7] K. Parodi, J.C. Polf, In vivo range verification in particle therapy, Med. Phys. 45 (11) (2018) 1036–1050.
[8] H. Paganetti, Range uncertainties in proton therapy and the role of Monte Carlo simulations, Phys. Med. Biol. 57 (11) (2012) 99–117.
[9] U. Schneider, E. Pedroni, A. Lomax, The calibration of CT Hounsfield units for radiotherapy treatment planning, Phys. Med. Biol. 41 (1) (1996) 111–124.
[10] N. Peters, P. Wohlfahrt, C.V. Dahlgren, L. de Marzi, M. Ellerbrock, F. Fracchiolla, J. Free, C. Gomà, J. Góra, M.F. Jensen, T. Kajdrowicz, R. Mackay, S. Molinelli, I. Rinaldi, V. Rompokos, D. Siewert, P. van der Tol, X. Vermeren, H. Nyström,

A. Lomax, C. Richter, Experimental assessment of inter-centre variation in stopping-power and range prediction in particle therapy, Radiother. Oncol. 163 (2021) 7–13.
[11] A. Meijers, J. Free, D. Wagenaar, S. Deffet, A.C. Knopf, J.A. Langendijk, S. Both, Validation of the proton range accuracy and optimization of CT calibration curves utilizing range probing, Phys. Med. Biol. 65 (3) (2020).
[12] E. Bär, A. Lalonde, G. Royle, H.M. Lu, H. Bouchard, The potential of dual-energy CT to reduce proton beam range uncertainties, Med. Phys. 44 (6) (2017) 2332–2344.
[13] F.K. Faller, S. Mein, B. Ackermann, J. Debus, W. Stiller, A. Mairani, Pre-clinical evaluation of dual-layer spectral computed tomography-based stopping power prediction for particle therapy planning at the Heidelberg Ion Beam Therapy Center, Phys. Med. Biol. 65 (9) (2020).
[14] P. Wohlfahrt, C. Möhler, C. Richter, S. Greilich, Evaluation of stopping-power prediction by dual- and single-energy computed tomography in an anthropomorphic ground-truth phantom, Int. J. Radiat. Oncol. Biol. Phys. 100 (1) (2018) 244–253.
[15] A.E. Bourque, J.F. Carrier, H. Bouchard, A stoichiometric calibration method for dual energy computed tomography, Phys. Med. Biol. 59 (8) (2014) 2059–2088.
[16] J.C. Polf, M.M. Mille, S. Mossahebi, H. Chen, P. Maggi, H. Chen-Mayer, Determination of proton stopping power ratio with dual-energy CT in 3D-printed tissue/air cavity surrogates, Med. Phys. 46 (7) (2019) 3245–3253.
[17] M. Simard, E. Bär, D. Blais, H. Bouchard, Electron density and effective atomic number estimation in a maximum a posteriori framework for dual-energy computed tomography, Med. Phys. 47 (9) (2020) 4137–4149.
[18] C. Shen, B. Li, L. Chen, M. Yang, Y. Lou, X. Jia, Material elemental decomposition in dual and multi-energy CT via a sparsity-dictionary approach for proton stopping power ratio calculation, Med. Phys. 45 (4) (2018) 1491–1503.
[19] Y. Xie, C. Ainsley, L. Yin, W. Zou, J. McDonough, T.D. Solberg, A. Lin, B.K. Teo, Ex vivo validation of a stoichiometric dual energy CT proton stopping power ratio calibration, Phys. Med. Biol. 63 (5) (2018).
[20] T. Näsmark, J. Andersson, Proton stopping power prediction based on dual-energy CT-generated virtual monoenergetic images, Med. Phys. 48 (9) (2021) 5232–5243.
[21] H. Bethe, J. Ashkin, in: E. Segré, J (Eds.), Experimental Nuclear Physics, Wiley, New York, 1953, p. 253.
[22] T. Flohr, M. Petersilka, A. Henning, S. Ulzheimer, J. Ferda, B. Schmidt, Photon-counting CT review, Phys. Med. 79 (2020) 126–136.
[23] M.J. Willemink, M. Persson, A. Pourmorteza, N.J. Pelc, D. Fleischmann, Photon-counting CT: technical principles and clinical prospects, Radiology 289 (2) (2018) 293–312.
[24] D.F. DeJongh, E.A. Dejongh, V. Rykalin, G. Defillippo, M. Pankuch, A.W. Best, G. Countrakon, K.L. Duffin, N.T. Karonis, C.E. Ordonez, C. Sarosiek, R.W. Schulte, J.R. Winans, A.M. Block, C.L. Hentz, J.S. Welsch, A comparison of proton stopping power measured with proton CT and x-ray CT in fresh postmortem porcine structures, Med. Phys. 48 (12) (2021) 7998–8009.
[25] A. Hammi, S. Koenigm D.C. Weber, B. Poppe, A.J. Lomax, Patient positioning verification for proton therapy using proton radiography, Phys. Med. Biol. 63 (2018) 24.
[26] M. Martišíková, T. Gehrke, S. Berke, G. Aricò, O. Jäkel, Helium ion beam imaging for image guided ion radiotherapy, Radiat. Oncol. 13 (1) (2018).
[27] M. Witt, U. Weber, D. Kellner, R. Engenhart-Cabillic, K. Zink, Optimization of the stopping-power-ratio to Hounsfield-value calibration curve in proton and heavy ion therapy, Z. Med. Phys. 25 (3) (2015) 251–263.
[28] F.K. Longarino, T. Tessonnier, S. Mein, S.B. Harrabi, J. Debus, W. Stiller, A. Mairani, Dual-layer spectral CT for proton, helium, and carbon ion beam therapy planning of brain tumors, J. Appl. Clin. Med. Phys. 23 (1) (2022).